Materials Advances

ROYAL SOCIETY OF CHEMISTRY

PAPER

View Article Online
View Journal | View Issue

Cite this: *Mater. Adv.*, 2024, 5, 1626

Development of magnetic nanoparticles with double silica shells of different porosities for efficient siRNA delivery to breast cancer cells

Qing Bao,[a] Xiangyu Liu,[a] Yan Li,[b] Tao Yang,[a] Hui Yue,[a] Mingying Yang *[b] and Chuanbin Mao *[c]

A nanosystem integrating silica and Fe_3O_4 faces multiple challenges in small interfering RNA (siRNA) delivery, such as inefficient loading of siRNA due to siRNA being a macromolecule compared to silica pore sizes and easy oxidation of Fe_3O_4 due to exposure to oxygen through the porous silica shell. To tackle these challenges, here we developed novel Fe_3O_4-based larger-pore silica-coated nanoparticles (FLSNs) by forming clusters of Fe_3O_4-based amorphous silica-coated nanoparticles (FASNs) first and then coating the clusters with a mesoporous silica shell with larger pores of ~6–50 nm. The densely-packed less-porous amorphous silica shell on the FASNs was designed to prevent the oxidation of the Fe_3O_4 cores, while the larger-pore mesoporous silica shell was intended for loading siRNA macromolecules. FLSNs were synthesized in three steps. Firstly, Fe_3O_4 nanoparticles with a super-paramagnetic magnetite structure were fabricated. Subsequently, amorphous silica was coated onto the surface of the Fe_3O_4 nanoparticles through a reverse-microemulsion method to obtain FASNs. Then, FASNs were aggregated into clusters in the emulsion system formed through ultrasonic treatment and a layer of larger-pore mesoporous silica was coated onto the surface of the FASN clusters to form FLSNs using mesitylene as a pore-swelling agent. The FLSNs were further employed as a novel siRNA delivery system for inducing cancer cell apoptosis. siRNA against polo-like kinase 1 (siPLK1) was delivered by FLSNs as a model siRNA, which could induce the apoptosis of triple-negative breast cancer cells (MDA-MB-231) upon efficient cellular uptake and endosome escape. After being modified with amino groups, the FLSNs not only show a significantly higher siRNA loading efficiency, but also can be efficiently taken up by MDA-MB-231 cells. The delivered siRNA could successfully enter the cellular cytoplasm and escape from endosomal entrapment to trigger cellular apoptosis. With the aid of an external magnetic field, the siRNA delivery efficiency was further enhanced, significantly reducing the viability of the breast cancer cells. Hence, the FLSNs are promising gene delivery carriers that can be used in gene therapy.

Received 19th August 2023,
Accepted 29th November 2023

DOI: 10.1039/d3ma00568b

rsc.li/materials-advances

Introduction

Gene therapy based on small interfering RNA (siRNA) is a promising technology to downregulate the genes for disease treatment.[1] However, it is difficult for the naked siRNA with large molecular weight and high negative charge to penetrate through the cellular membrane. Moreover, siRNA is unstable and can be easily degraded by the enzymes in the complex physiological microenvironment. Thereby, an efficient siRNA delivery system is crucial for successful RNA interference (RNAi) therapy.

In the past decade, various delivery systems have been explored including lipid nanoparticles,[2,3] viruses,[4,5] and ligand-conjugated siRNAs.[6,7] Among all of these, mesoporous silica nanoparticles have drawn much attention from researchers due to their unique characteristics.[8,9] Mesoporous silica nanoparticles have a tunable porous structure and can be modified with various functional groups.[10] Additionally, silica can be coated onto the surface of many inorganic nanoparticles to form multifunctional core–shell nanoparticles. This unique property makes it possible to develop a vast array of nanomaterials in the area of siRNA delivery. Furthermore, the advantages of using mesoporous silica nanoparticles for siRNA delivery include multiple aspects. Firstly, their tunable porous structure allows for precise control over siRNA loading and release kinetics, which is crucial for achieving therapeutic efficacy, while minimizing side effects. Moreover, the combination of mesoporous silica nanoparticles with other inorganic

[a] School of Materials Science and Engineering, Zhejiang University, 310058, China
[b] College of Animal Science, Zhejiang University, 310058, China. E-mail: yangm@zju.edu.cn
[c] Department of Biomedical Engineering, The Chinese University of Hong Kong, Sha Tin, Hong Kong SAR, China. E-mail: cmao@cuhk.edu.hk

nanoparticles, such as Fe_3O_4 nanoparticles, offers multifunctional core–shell nanoparticles that can facilitate magnetic targeting,[11,12] magnetic-heat therapy and magnetic resonance imaging.[13] The incorporation of magnetic properties allows for precise guidance of the nanoparticles to the tumor site using an external magnetic field, enhancing the delivery efficiency of siRNA. This approach, known as magnetofection,[14] holds great promise for improving the precision and effectiveness of siRNA-based cancer therapy.

However, there are still some limitations of silica-based delivery systems. For instance, the typical pore size of traditional mesoporous silica nanoparticles ranging from 2 to 5 nm is not favorable for the encapsulation of macromolecular agents including siRNA ($\approx$13 kDa).[15] Additionally, some reported magnetic silica-based nanoparticles are so large ($>$200 nm) that they cannot be effectively taken up by target cells.[16,17] Moreover, almost all magnetic silica-based nanoparticles were fabricated through coating porous silica directly onto the surface of Fe_3O_4 nanoparticles. The porous structure of the silica shell may cause direct contact between the air and Fe_3O_4, resulting in oxidation of the Fe_3O_4 core. Therefore, developing an effective and appropriate siRNA delivery system remains a big challenge.

Herein, monodispersed Fe_3O_4-based larger-pore mesoporous-silica-coated nanoparticles (FLSNs) with a size less than 200 nm are successfully developed to bear two silica shells and applied as a novel siRNA delivery carrier (Fig. 1). Fe_3O_4-based amorphous silica nanoparticles (FASNs) were first synthesized and then aggregated into a cluster in the emulsion system formed by ultrasonic treatment. Then larger-pore mesoporous silica shells were coated onto FASN clusters, generating FLSNs. Finally, the FLSNs were functionalized with cationic amino groups to favor the loading of anionic siRNA. The hydroxyl groups on the surface of the silica shell could be conjugated with 3-aminopropyltriethoxysilane (APTES) to make FASNs bear amino groups. The FLSNs were designed to have multiple desired advantages. First, in the cluster of FASNs, an amorphous silica shell is coated on the Fe_3O_4 core, preventing the Fe_3O_4 cores in FLSNs from being oxidized. Second, FLSNs have a mesoporous silica shell with a pore size of $\sim$6–50 nm and a large surface-area-to-volume ratio, favoring the trapping of macromolecular siRNA into their pore structure. Third, the large mesoporous structure can effectively protect siRNA against enzymatic degradation. Fourth, FLSNs with appropriate particle sizes can be taken up by the cells, followed by successful endosome escape. Fifth, the magnetic core is super-paramagnetic, allowing us to add an external magnet to facilitate siRNA's cellular uptake and delivery. Finally, the FLSNs have good cellular biocompatibility.

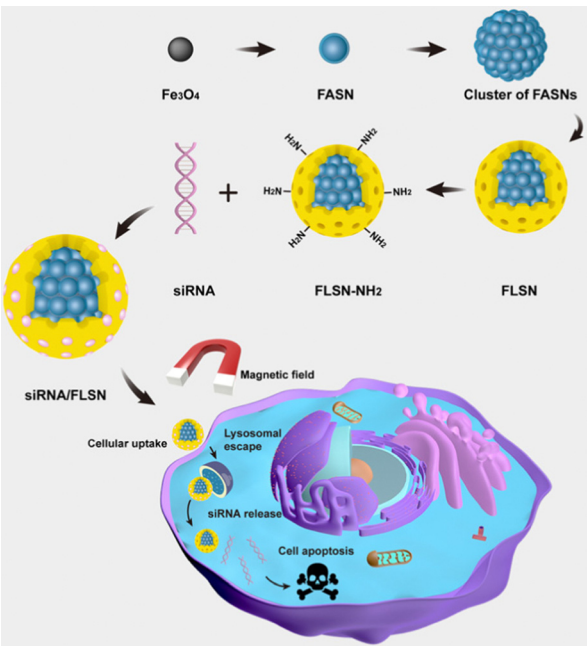

Fig. 1 Schematic illustration of the fabrication and mechanism of the siRNA/FLSNs complex for RNAi therapy.

In this study, FLSNs were used to deliver the siRNA against polo-like kinase 1 (siPLK1) into triple-negative breast cancer cells (MDA-MB-231) to induce cellular apoptosis. siPLK1 (AGAU CACCCUCCUUAAAUAUUdTdT) could downregulate polo-like kinase 1, which leads to mitotic arrest and cellular apoptosis.[18] With the aid of an external magnetic field, FLSNs can successfully trigger the apoptosis of MDA-MB-231 through the effective delivery of siPLK1 (Fig. 1). We believe that the successful construction of the magnetic silica delivery system offers a paradigm for the development of cancer gene therapy.

Results and discussion

Synthesis and characterization of nanoparticles

The magnetic Fe_3O_4 nanoparticles were first prepared through a previously reported method.[19] From the transmission electron microscopy (TEM) image, the Fe_3O_4 nanoparticles are spherical, uniform and monodispersed with a particle size of about 20 nm (Fig. 2B). Subsequently, amorphous silica was coated onto the surface of the Fe_3O_4 nanoparticles through a reverse-micro-emulsion method, generating hydrophilic core–shell Fe_3O_4@amorphous silica nanoparticles (termed FASN) with a size of $\sim$30 nm (Fig. 2C). Each FASN has a single Fe_3O_4 core. Then, a layer of larger-pore mesoporous silica enveloped the cluster of as-synthesized FASNs, forming Fe_3O_4-based larger-pore silica nanoparticles (FLSNs). During this process, mesitylene (TMB), as a pore-swelling agent, was added into the solution of cetyltrimethylammonium chloride (CTAC)-stabilized FASNs, allowing CTAC and TMB to form CTAC–TMB aggregates. Compared with CTAC micelles, the CTAC–TMB aggregates could largely increase the pore size of the silica shell in the typical silica sol–gel reaction (Fig. 2A). The TEM image in Fig. 2D shows that the obtained FLSNs are uniform, monodisperse and sunflower-shaped with a particle size of about 150 nm. The scanning transmission electron microscopy (STEM) image and elemental mapping images further verified the core–shell structure of the FLSNs (Fig. 2E–H).

Moreover, the crystal phase of the nanoparticles was confirmed *via* X-ray diffraction (XRD) to be the inverse cubic spinel structure of magnetite (JCPDS no. 79-0416) (Fig. 3A). This result suggested that the crystal phase of the Fe_3O_4-core did not change during the process of coating silica. Additionally, the

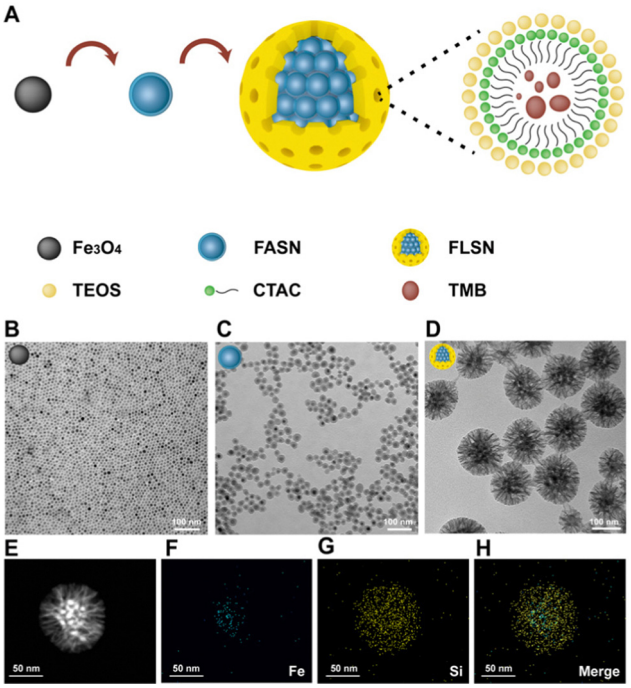

Fig. 2 The design and preparation of FLSNs. (A) Schematic of the preparation of the FLSNs. At first, Fe_3O_4 nanoparticles were fabricated and dispersed in an organic solvent. Subsequently, amorphous silica was coated onto the surface of the Fe_3O_4 nanoparticles, resulting in Fe_3O_4-based amorphous silica nanoparticles (FASNs). Finally, larger-pore mesoporous silica enveloped the cluster of FASNs, forming Fe_3O_4-based larger-pore silica nanoparticles (FLSNs). In this process, TMB served as a pore-swelling agent to form a larger CTAC–TMB aggregate. (B)–(D) The TEM images of the Fe_3O_4 nanoparticles (B), FASNs (C), and FLSNs (D). (E) The STEM image of the FLSNs. (F)–(H) The elemental mapping of the FLSNs, including Fe (F), Si (G), and the merged image (H).

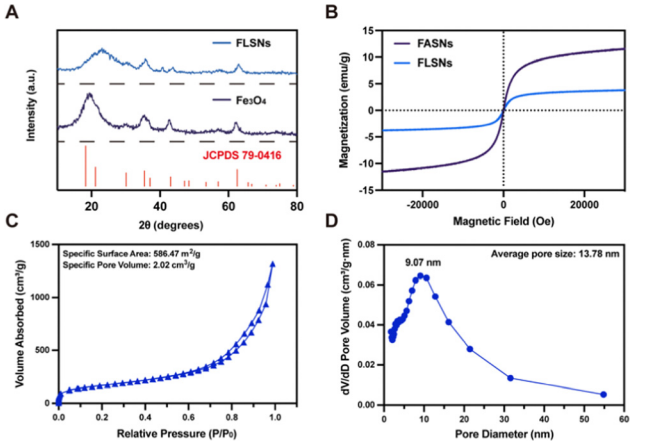

Fig. 3 The characterization and properties of the obtained nanoparticles. (A) XRD patterns of FASNs (blue) and Fe_3O_4 nanoparticles (purple), which could be well indexed to Fe_3O_4 (JCPDS 79-0416). (B) VSM magnetization curves of FLSNs (blue) and FASNs (purple). (C) Nitrogen adsorption/desorption isotherms of FLSNs. (D) Pore size distribution of FLSNs.

magnetic properties of the nanoparticles were investigated using a vibrating sample magnetometer (VSM) (Fig. 3B). Both FASNs and FLSNs exhibited excellent super-paramagnetic properties with no hysteresis in low fields. The saturation magnetization of the FLSNs (3.76 emu g^{-1}) is lower than that of FASNs (11.58 emu g^{-1}) due to the larger weight fraction of silica in the former.

The porous structure of the FLSNs was analyzed through Brunauer–Emmett–Teller (BET) measurements. The specific surface area and specific pore volume of the FLSNs were calculated to be 586.47 m^2 g^{-1} and 2.02 cm^3 g^{-1}, respectively (Fig. 3C), which are much larger than several large-mesoporous core–shell nanoparticles reported previously.[15,20] Specifically, the average pore size of the FLSNs was 13.78 nm, which was larger than reported mesoporous silica. In the meantime, the pore size distribution of FLSNs is broadened, which is due to the pore-swelling effect of TMB (Fig. 3D).

Loading/release behavior and protection of siRNA

The FLSNs were subsequently aminated *via* grafting 3-aminopropyltriethoxysilane (APTES) to present positive charges on their surface. The aminated FLSNs were then allowed to interact with negatively charged siRNA to absorb and load siRNA through electrostatic interaction. To investigate the loading capacity of FLSNs, siRNA was incubated with different amounts of FLSNs with the weight ratio (FLSNs : siRNA) increasing from 0 to 300. After centrifugation, the supernatants were analyzed using an agarose gel retardation assay. As shown in Fig. 4A, the amounts of siRNA in the supernatants were gradually decreased as the FLSN to siRNA weight ratio increased. When the weight ratio of FLSNs : siRNA was above 50, siRNA was completely loaded into FLSNs and the siRNA in the supernatant completely disappeared, suggesting a loading capability of around 2 wt%. To further confirm the excellent siRNA loading capacity, zeta potentials of the siRNA-loaded FLSNs (denoted as siRNA/FLSNs) were measured (Fig. 4B). The zeta potential values of the siRNA/FLSNs were gradually elevated as the weight ratio of FLSNs : siRNA increased. When the weight ratio of FLSNs : siRNA reached 50, the zeta potential value of the siRNA/FLSNs was close to zero, which was consistent with the result of agarose gel electrophoresis assay. These data taken together indicated that FLSNs could efficiently load siRNA and the loading ratio of siRNA/FLSNs was fixed at 50 for all subsequent assays.

There are many endonucleases in physiological fluids, which can easily degrade siRNA. Therefore, the delivery of siRNA should protect siRNA against degradation. To evaluate the siRNA protective capacity of FLSNs, the siRNA/FLSNs complex was treated with different amounts (5, 10, and 20 mU) of ribonuclease A (RNase) for 1 h. After RNase-treatment, the samples were centrifuged and treated with heparin to release the surviving siRNA into the supernatant. It was found that the siRNA/FLSN complex could effectively defend the degradation of 20 mU RNase (Fig. 4C), suggesting a good siRNA protection performance of FLSNs. The release behavior of siRNA from the siRNA/FLSN complex was further investigated (Fig. 4D). The siRNA/FLSN complex was dispersed in acidic (pH = 5.0) and neutral (pH = 7.4) buffer solutions. After 24 h and 48 h of incubation, the siRNA/FLSNs were collected through centrifugation and treated with heparin to release the loaded siRNA. As shown in Fig. 4D, siRNA was preferentially released from the

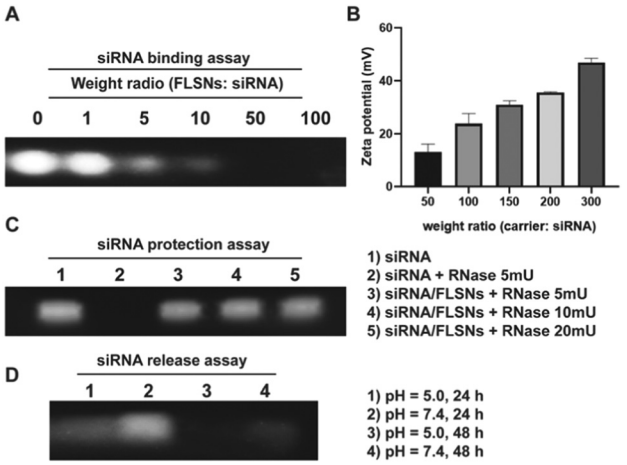

Fig. 4 Binding of siRNA by FLSNs and release of siRNA from FLSNs. (A) Agarose gel retardation assay of the supernatant of siRNA solution after incubation with FLSNs at various weight ratios of FLSNs/siRNA. (B) The zeta potential values of the FLSNs/siRNA complex at various weight ratios of FLSNs/siRNA. (C) The protective effect of siRNA by FLSNs against RNase digestion. After incubation with RNase, the residual siRNA was released from FLSNs through heparin treatment and analyzed using an agarose gel retardation assay. (D) The release behaviors for siRNA from the FLSNs/siRNA complex under acidic (pH = 5) and neutral (pH = 7.4) conditions. After 24 h or 48 h incubation, the residual siRNA was released from the FLSNs through heparin treatment and analyzed using the agarose gel retardation assay.

siRNA/FLSN complex in the acidic medium instead of in the neutral medium. After 48 h of incubation in acidic conditions, the loaded siRNA was completely released, which is evidenced through the disappearance of siRNA bands. Considering the acidic microenvironment in the tumor, this pH-responsive release behavior is favorable for tumor-targeted siRNA delivery.

Cellular delivery of siRNA

In order to investigate the cellular delivery of siRNA, fluorescein isothiocyanate (FITC)-labeled siRNA was synthesized and loaded into FLSNs to form FITC-FLSNs. Subsequently, the FITC-FLSNs were incubated with the triple-negative breast cancer MDA-MB-231 cell line with or without a magnetic field. After free siRNA was removed by washing, the cells were fluorescently analyzed *via* confocal microscopy. Compared to the cells without a magnetic field, stronger green fluorescence was observed in the cells that were cultured under a magnetic field (Fig. 5A). This enhanced cellular uptake could be attributed to the magnetic driving of the FITC-FLSNs towards the cellular surface.

Another critical challenge of siRNA delivery is endosomal entrapment. It is necessary for the delivered siRNA to escape from endosomes without degradation. To assess the endosomal escape capacity of siRNA/FLSNs, the subcellular location of endosomes and siRNA/FLSNs was observed using confocal microscopy (Fig. 5B). After 6 h of incubation, the siRNA signal (green) and the endosome signal (red) were not co-localized, demonstrating the successful endosome escape of the FLSN-delivered siRNA. Additionally, little colocalization of the green and red signals was also observed in a few cells, indicating that the siRNA/FLSNs were going through an endocytosis pathway.

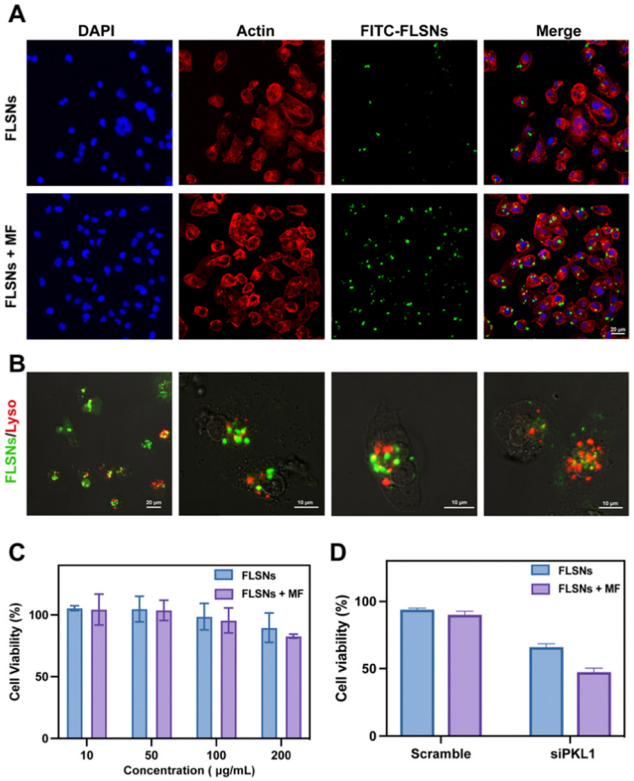

Fig. 5 Viability of MDA-MB-231 cancer cells after interaction with FLSNs: (A) confocal fluorescence images of MDA-MB-231 cells incubated with FITC-labeled FLSNs with or without a magnetic field (MF). (B) Confocal fluorescence images of the subcellular location of endosomes (red) and siRNA/FLSNs (green). (C) Relative cell viability of MDA-MB-231 cells co-cultured with various concentrations (10, 50, 100, and 200 μg mL^{-1}) of FLSNs for 48 h. (D) Relative cell viability of MDA-MB-231 cells after incubation with siRNA/FLSNs complex loading siPKL1 or scramble siRNA with (purple) or without (blue) a magnetic field.

Cytotoxicity and siRNA delivery function of FLSNs

To evaluate the cytotoxicity of FLSNs, a standard cell counting kit-8 (CCK-8) assay was performed on MDA-MB-231 cell lines. Various concentrations of FLSNs were incubated with the cells for 48 h. The MDA-MB-231 cell viability was not significantly affected even under the concentration of up to 200 μg mL^{-1} (Fig. 5C). Additionally, the FLSNs also exhibited negligible toxicity towards MDA-MB-231 cells in the presence of an external magnetic field. The low cytotoxicity and good biocompatibility of the FLSNs are desired in the applications of intracellular delivery.

Next the functional siRNA delivery was further investigated. To verify the RNA interference therapy effect of siRNA/FLSNs, siRNA with a scrambled sequence was synthesized as a negative control (denoted as scramble) (Fig. 5D). The cell viability decreased to 65% when the siPLK1 was delivered into MDA-MB-231 cells through the siRNA/FLSN complex. However, the MDA-MB-231 cells treated with scramble-loaded FLSNs had no obvious cell death. This result suggests that the siRNA/FLSN complex could deliver siPKL1 into the MDA-MB-231 cells to achieve RNA interference therapy. In addition, a marked drop was observed in the cell viability when a magnetic field was

applied. The increased inhibition effect could be explained by the enhanced cellular uptake of siRNA-loaded FLSNs with the help of an external magnetic field.

The successful siRNA delivery results from the unique properties of FLSNs including high siRNA loading capacity, effective siRNA protection, and excellent cellular viability. In a study reported previously,[15] the surface area and the pore volume of large-mesoporous Fe_3O_4@SiO_2 nanoparticles were calculated to be 411 $m^2\ g^{-1}$ and 1.13 $cm^3\ g^{-1}$ (both lower than those of FLSNs), respectively. In the meantime, the large-mesoporous Fe_3O_4@SiO_2 nanoparticles reported previously could only protect the loaded siRNA against 5 mU of RNase.[15] From the results above, FLSNs with high surface area and pore volume can effectively protect the loaded siRNA against 20 mU of RNase. Thereby, the FLSNs are a potential siRNA delivery vehicle to achieve successful RNAi therapy.

Conclusions

In conclusion, novel monodisperse magnetic larger-pore mesoporous silica-coated Fe_3O_4 nanoparticles (FLSNs) have been successfully fabricated. These nanoparticles exhibit a large surface-area-to-volume ratio, a high pore volume, and magnetization. After surface modification of amino groups, the FLSNs could effectively load siRNA into their porous structures and protect siRNA against enzymatic degradation. By loading siPKL1 as RNAi therapeutic agents, the siRNA/FLSN nanocomplex could enter the cytoplasm of triple-negative breast cancer cells (MDA-MB-231) and escape endosomal entrapment. Furthermore, with the aid of an external magnetic field, the siRNA/FLSN nanocomplex could effectively trigger the apoptosis of MDA-MB-231 cancer cells because of highly efficient siRNA delivery. These results indicate that the above multifunctional FLSNs have great potential for siRNA therapeutic applications and thus their *in vivo* use remains to be studied. We believe that the successful construction of magnetic silica nanoparticles could provide a paradigm for the development of siRNA delivery systems and trigger excitement in further exploring the multifunctionality of these nanoparticles such as magnetic targeting, magnetic-heat therapy and magnetic resonance imaging.

Conflicts of interest

There are no conflicts to declare.

Acknowledgements

M.Y. acknowledges the support of Zhejiang Provincial Science and Technology Plan (2021C02072-6), the National Natural Science Foundation of China (81871482, 81871499, 81911530223, and 32101095), Provincial Key Laboratory Construction Plans (2020E10025), State of Sericulture Industry Technology System (CARS-18-ZJ0501), and Plan of National and Zhejiang Provincial Youth Science and Technology Innovation leader ([2020]366 and 2018R52021).

References

1 D. Lu and T. Thum, *Nat. Rev. Cardiol.*, 2019, **16**, 661–674.
2 J. A. Kulkarni, P. R. Cullis and R. van der Meel, *Nucleic Acid Ther.*, 2018, **28**, 146–157.
3 J. A. Kulkarni, D. Witzigmann, S. Chen, P. R. Cullis and R. van der Meel, *Acc. Chem. Res.*, 2019, **52**, 2435–2444.
4 P. Lam and N. F. Steinmetz, *Biomater. Sci.*, 2019, **7**, 3138–3142.
5 R. Guagliardo, L. Herman, J. Penders, A. Zamborlin, H. De Keersmaecker, T. Van de Vyver, S. Verstraeten, P. Merckx, M. P. Mingeot-Leclercq, M. Echaide, J. Pérez-Gil, M. M. Stevens, S. C. De Smedt and K. Raemdonck, *ACS Nano*, 2021, **15**, 8095–8109.
6 H. Du Rietz, H. Hedlund, S. Wilhelmson, P. Nordenfelt and A. Wittrup, *Nat. Commun.*, 2020, **11**, 1809.
7 T. Harumoto, H. Iwai, M. Tanigawa, T. Kubo, T. Atsumi, K. Tsutsumi, M. Takashima, G. Destito, R. Soloff, K. Tomizuka, C. Nycholat, J. Paulson and K. Uehara, *ACS Chem. Biol.*, 2022, **17**, 292–298.
8 R. Heidari, P. Khosravian, S. A. Mirzaei and F. Elahian, *Sci. Rep.*, 2021, **11**, 20531.
9 Y. Song, B. Zhou, X. Du, Y. Wang, J. Zhang, Y. Ai, Z. Xia and G. Zhao, *Biomed. Pharmacother.*, 2020, **125**, 109561.
10 Y. Wang, Y. Xie, K. V. Kilchrist, J. Li, C. L. Duvall and D. Oupický, *ACS Appl. Mater. Interfaces*, 2020, **12**, 4308–4322.
11 Y. Guan, Y. Yang, X. Wang, H. Yuan, Y. Yang, N. Li and C. Ni, *J. Mol. Liq.*, 2021, **327**, 114783.
12 N. Gandra, D.-D. Wang, Y. Zhu and C. Mao, *Angew. Chem., Int. Ed.*, 2013, **52**, 11278–11281.
13 N. Kurnaz Yetim, F. Kurşun Baysak, M. M. Koç and D. Nartop, *J. Mater. Sci.: Mater. Electron.*, 2020, **31**, 18278–18288.
14 Q. Bi, X. Song, A. Hu, T. Luo, R. Jin, H. Ai and Y. Nie, *Chin. Chem. Lett.*, 2020, **31**, 3041–3046.
15 L. Xiong, J. Bi, Y. Tang and S.-Z. Qiao, *Small*, 2016, **12**, 4735–4742.
16 Q. Yue, J. Li, W. Luo, Y. Zhang, A. A. Elzatahry, X. Wang, C. Wang, W. Li, X. Cheng, A. Alghamdi, A. M. Abdullah, Y. Deng and D. Zhao, *J. Am. Chem. Soc.*, 2015, **137**, 13282–13289.
17 D. Niu, Z. Liu, Y. Li, X. Luo, J. Zhang, J. Gong and J. Shi, *Adv. Mater.*, 2014, **26**, 4947–4953.
18 G. Kuang, H. Lu, S. He, H. Xiong, J. Yu, Q. Zhang and Y. Huang, *Adv. Healthcare Mater.*, 2021, **10**, 2100938.
19 J. Park, K. An, Y. Hwang, J.-G. Park, H.-J. Noh, J.-Y. Kim, J.-H. Park, N.-M. Hwang and T. Hyeon, *Nat. Mater.*, 2004, **3**, 891–895.
20 B. Ding, S. Shao, C. Yu, B. Teng, M. Wang, Z. Cheng, K.-L. Wong, P. A. Ma and J. Lin, *Adv. Mater.*, 2018, **30**, 1802479.